Title

RELIABLE IDENTIFICATIONS OF ACTIVE GALACTIC NUCLEI FROM THE WISE, 2MASS, AND ROSAT ALL-SKY SURVEYS

Journal

The Astrophysical Journal, 751(1)

ISSN

0004-637X

Authors

Edelson, R
Malkan, M

Publication Date

2012-05-20

DOI

10.1088/0004-637x/751/1/52

Peer reviewed

Accepted for publication by the Astrophysical Journal

Reliable Identifications of AGN from the WISE, 2MASS and Rosat all-sky surveys

Short title: AGN from all-sky surveys

R. Edelson [1, 2] & M. Malkan [3]

ABSTRACT

We have developed the "S_{IX}" statistic to identify bright, highly-likely Active Galactic Nucleus (AGN) candidates solely on the basis of WISE, 2MASS and Rosat all-sky survey data. This statistic was optimized with data from the preliminary WISE survey and the SDSS, and tested with Lick 3-m Kast spectroscopy. We find that sources with $S_{IX} < 0$ have a $\gtrsim$95% likelihood of being an AGN (defined in this paper as a Seyfert 1, quasar or blazar). This statistic was then applied to the full WISE/2MASS/RASS dataset, including the final WISE data release, to yield the "W2R" sample of 4,316 sources with $S_{IX} < 0$. Only 2,209 of these sources are currently in the Veron-Cetty and Veron (VCV) catalog of spectroscopically confirmed AGN, indicating that the W2R sample contains nearly 2,000 new, relatively bright (J $\lesssim$ 16) AGN.

We utilize the W2R sample to quantify biases and incompleteness in the VCV catalog. We find it is highly complete for bright (J < 14), northern AGN, but the completeness drops below 50% for fainter, southern samples and for sources near the Galactic plane. This approach also led to the spectroscopic identification of 10 new AGN in the Kepler field, more than doubling the number of AGN being monitored by Kepler. This has identified ~1 bright AGN every 10 square degrees, permitting construction of AGN samples in any sufficiently large region of sky.

Subject headings: Astronomical databases: surveys -- Galaxies: active -- Galaxies: Seyfert -- Methods: statistical -- Quasars: general

1. Introduction

Surveys for active galactic nuclei[4] (AGN), or extragalactic objects in general, have at least one of two broad goals: first, they can constrain the space densities and redshift-evolution of sources, providing key inputs to cosmological models. This requires a high level of completeness, or at least clear understanding of bias and incompleteness.

Second, such surveys often produce new samples of AGN useful for follow-up studies. For example, early AGN surveys (e.g., the 3C radio survey [Edge et al. 1959] and the ultraviolet-excess/spectroscopy surveys of Markarian et al. 1989 and Green et al. 1986) identified bright AGN that have subsequently been observed in many ways and at many wavelengths, providing key constraints on AGN and black hole physics. (Of course, those surveys have also made important contributions in their own right, on questions such as, e.g., AGN evolution.) Some AGN turn out to be of special value because of their location in the sky (e.g., near the ecliptic poles, and thus in the continuous viewing zone of some satellites) or due to their angular

[1] Department of Astronomy, University of Maryland, College Park, MD 20742-2421
[2] e-mail: rickedelson@gmail.com; phone: 970-531-3748
[3] Department of Physics and Astronomy, University of California Los Angeles, Los Angeles, CA 90095-1547

[4] In this paper, the term AGN refers only to objects with broad permitted emission lines (Seyfert 1-1.9 galaxies and quasars) or highly polarized objects (BL Lac objects and highly-polarized quasars), and not to narrow-line objects such as Seyfert 2 galaxies, LINERs and starburst galaxies.

proximity to foreground galaxies (for absorption line studies), or to bright stars (for adaptive optics studies). For all of these purposes, completeness is not as important as the ability to confidently identify bright AGN throughout the sky.

In particular it would be useful to be able to construct a sample of AGN in any sufficiently large region of the sky, even if it has not been subjected to any spectroscopic surveys. That capability has until now been lacking. For example, the Kepler mission (Boruki et al. 2010) can produce unprecedented optical AGN light curves (e.g., Mushotzky et al. 2011), but it wasn't until after ~1.5 years of the mission had elapsed that a significant number of AGN in the Kepler field had been identified and monitoring begun.

This paper presents a method to identify AGN candidates solely on the basis of data from the Wide-field Infrared Survey Explorer (WISE; see Wright et al. 2010), the 2-Micron All-Sky Survey (2MASS; Skrutzkie et al. 2006) and the Rosat All-Sky Survey (RASS; Voges et al. 1999). It is arranged as follows: the next section presents the derivation of the S_{IX} statistic to identify highly-likely AGN candidates from the preliminary WISE/2MASS/RASS data, and its initial optimization with Sloan Digital Sky Survey release 8 data (SDSS-8; York et al. 2000). Section 3 reports spectroscopic observations of new AGN candidates used to test the statistic, resulting in a catalog of highly-likely (≳95% confidence) AGN candidates across the sky. It also analyzes its effectiveness in terms of the intrinsic infrared and X-ray properties of AGN. Section 4 applies this statistic to the full WISE/2MASS/RASS data to derive the "W2R" catalog, and utilizes this sample to address a number of questions including the relative frequency of blazars, the completeness of the Veron-Cetty & Veron (2006; VCV hereafter) AGN catalog, and identification of new AGN in the Kepler field. Section 5 gives a brief concluding discussion. An Appendix presents an alternate AGN statistic that does not require detection in RASS, and the associated "W2" sample designed to maximize AGN completeness instead of reliability.

2. Method

2.1. Overview

AGN have distinctive continuum emission in both the infrared and X-ray bands. Few other sources emit strongly all the way from 1.2 to 22 μm (the full range of the WISE/2MASS data), and those that do have different colors from AGN. That is, it has been known for several decades that AGN have near- to mid-IR spectral energy distributions (SEDs) resembling a power law with a typical slope of $F_\nu \propto \nu^{-1}$ (Edelson & Malkan 1986). On the other hand, normal galaxies – stars plus cool dust – show ``bumpier" SEDs dominated by starlight shortwards of 5 μm, and by cooler dust continuum and PAH bands from ~7 to 20 μm.

Likewise it appears that almost all AGN can be detected in the X-rays with sufficiently long integrations. For instance, ~80% of the 12 μm Seyfert 1s were detected in the RASS (Rush et al. 1996) even though the effective integration times were short (typically a few hundred seconds), and the remainder were detected in longer (~10 ks) pointed Rosat observations (Rush & Malkan 1996). These characteristics – distinctive infrared colors and X-ray detectability – make it possible to identify bright AGN solely on the basis of WISE, 2MASS and RASS data.

In this analysis, we are testing the null hypothesis that an object is not an AGN. All statistical tests such as this involve a tradeoff between Type I errors (incorrectly rejecting the null hypothesis when true, i.e. a ‘false positive’ inclusion of an object which is not a true AGN), and Type II errors (incorrectly accepting the null hypothesis when false; i.e., a ‘false negative’,

where a true AGN is incorrectly excluded; see Fisher, 1935 for details). Because we are primarily interested in high reliability, our approach minimizes the Type I error rate (contamination from inclusion of non-AGN), at the expense of a large (and ill-defined) Type II error rate (failure to include other real AGN). That is, we are willing to tolerate a high degree of incompleteness in order to maximize our confidence in our AGN identifications. (A complementary approach that minimizes Type II errors at the expense of a higher Type I error rate is given in Appendix A.) Our statistic was empirically constructed by combining infrared colors and distance to the nearest X-ray source. A low value of the resulting S_{IX} index indicates an object with AGN-like 2–20 μm continuum and likely X-ray emission, corresponding to a high likelihood of being an AGN.

2.2. Defining the samples

To construct and test the AGN statistic, we begin by defining three test samples. First, we restricted ourselves to the 83,510 objects detected at 10σ or better in all four WISE (3.4, 4.6, 12, 22 μm) and all three 2MASS (1.2, 1.6, 2.2 μm) bands. This sample can be obtained by issuing the SQL command "w1mpro > 9 and w1snr > 10 and w2snr > 10 and w3snr > 10 and w4snr > 10 and n_2mass = 1 and j_msig_2mass < 0.1 and h_msig_2mass < 0.1 and k_msig_2mass < 0.1" to the WISE Preliminary Release Source Catalog on the page http://irsa.ipac.caltech.edu/cgi-bin/Gator/nph-scan. Note that the first part of the command removes sources with W1 < 9 magnitudes. As discussed in Section 4.1, this eliminates ~0.5% of the brightest AGN but nearly half of the stars, because very few AGN are brighter than W1 = 9.

WISE/2MASS associations are taken from the WISE preliminary database; in order to be included the separation must be less than 3" (see http://wise2.ipac.caltech.edu/docs/release/prelim/expsup/sec4_7.html#2mass_assoc for details). For each object, we also measured the angular distance from the WISE position to the nearest RASS source. We call this the "full" sample because it contains data on all currently available sources with good detections with both WISE and 2MASS.

In order to optimize the test statistic, we require a second sample of objects that have optical identification spectra. We utilize a subsample of the 4,954 WISE/2MASS/RASS sources that also have SDSS-8 spectra. We refer to this as the "SDSS" sample. It is not a purely random sampling of the WISE/2MASS/RASS candidates, because SDSS was most focused on observing (often unusual) galaxies. Relative to the full WISE sample, stars and "normal" spiral galaxies are underrepresented in the SDSS sample, while X-ray-bright galaxies (often AGN) are overrepresented.

The testing and validation also require a third subsample, containing just the sources identified as AGN in the SDSS sample. To produce this, we visually examined each of the 797 spectra with SDSS class=QSO, isolating a sample of 741 with Seyfert 1/quasar spectra. We refer to the 741 true broad-line active galaxies as the "lines=B" sample because these sources all exhibit broad emission lines. The remaining 46 class=QSO sources turned out to be narrow-line objects, e.g., Seyfert 2s. They had Hα emission lines mistakenly identified as "broad" due to poor automated continuum fitting, e.g. around the atmospheric absorption in the B band. More generally, the other 4,157 SDSS sources were a combination of galaxies and stars.

2.3. Constructing the infrared color discriminator

The next step is to utilize these samples to construct a statistic that picks out AGN on the basis of their infrared colors. The first three rows of Figure 1 compare histograms of the five

measured infrared colors (J-H, H-K, W1-W2, W2-W3, W3-W4) for each of these three samples. (Following Wright et al. 2010, WISE bands centered at 3.4, 4.6, 11.6 and 22 μm are denoted W1, W2, W3 and W4, respectively.) The bottom row gives *R*, the ratio of the number of lines=B objects to the total number of SDSS objects in each color bin. For a given color bin, a value of *R* = 1 would mean that all of the sources in that bin are broad-line AGN, while *R* = 0 would indicate that all are non-AGN. Thus, *R* is a differential likelihood indicator that a source with a given color is an AGN.

The colors H-K, W1-W2, and W2-W3 show the largest range in *R*. (The underlying physical reason for this, discussed in Section 2.1., is that AGN have power-law infrared SEDs, while the infrared SEDs of normal galaxies are made up of multiple components, and the power-law is not that dissimilar from starlight in J-H and cool dust in W3-W4.) This is also apparent in Table 1: the AGN and non-AGN show very similar mean J-H and W3-W4 colors, while they are very different in the other three colors. Because of this, we formed our AGN template on the basis of the three colors H-K, W1-W2 and W2-W3, and ignored J-H and W3-W4.

Figure 1 reveals further important details of these color discriminators. Note that for W2-W3, the ratio *R* shows a fairly narrow and well-defined peak centered near ~2.93. We define a parameter to score how "AGN-like" that color is for each source, as follows:

$$c_4 = \mathrm{abs}(2.93-(W2-W3)),$$

where abs refers to the absolute value function. A small value of c4 indicates a W2-W3 color close to the "optimal" value of 2.93, and a large value indicates a highly-discrepant value. Thus the smaller the score, the more likely this source is to be an AGN.

The parameter *R* behaves differently for H-K and W1-W2: in these cases, *R* increases to redder colors, with relatively broad transitions starting around ~0.77 and ~0.91, respectively. Thus for these two colors, we use a different functional form for the scoring parameter:

$$c_2 = \max(0.77-(H-K),0),$$

$$c_3 = \max(0.91-(W1-W2),0),$$

where max refers to the maximum function. That is, for H-K (W1-W2), any color redder than 0.77 (0.91) yields c2 (c3) = 0, while colors bluer than these receive increasingly positive scores, I e., higher penalties. Note that by design, the sense of all three "penalty functions" is the same: a low score indicates an AGN-like color and a high score indicates a non-AGN-like color, and all are positive-definite.

The observed AGN-like colors in each of these wavebands (Column 8 of Table 1) are very close to those that would have been expected from previous infrared photometry of well-known Seyfert 1 galaxies. Since the WISE and 2MASS magnitudes are on the Vega system, H-K = 0.77, W1-W2 = 0.91 and W2-W3 = 2.69 correspond to power-law slopes of approximately -1.07 from 1.66 μm to 2.16 μm, -0.80 between 3.4 and 4.6 μm, and -0.85 from 4.6 to 11 μm (see Table 1 in Wright et al. 2010). The near- to mid-infrared continua of Seyfert 1 nuclei are typically described by a ν^{-1} power-law. However, there are generally additional components present which alter the broadband colors, particularly starlight from the host galaxy which peaks at 1.6 μm, and a broad 3-5 μm ``bump" which makes the observed 3-12 μm slope significantly flatter (c.f. Edelson and Malkan 1986). The threshold colors we adopt encompass the mean AGN continuum shapes, as well as much of the cosmic scatter from one AGN to another.

Other groups have also used the approximate power-law shape of the AGN mid-IR continuum to select them, for example using 3.6—8um photometry from Spitzer/IRAC (Lacy et al. 2006, Stern et al. 2005). The idea that a red W1-W2 color measured by WISE should be a powerful selector for AGN was explicitly anticipated by Assef et al. (2010).

2.4. Optimizing the infrared color discriminator

Next, these scores are combined to produce a statistic with the same sense: a low score indicates a high likelihood that the source is an AGN, and the result is positive-definite. This is done by forming a linear combination of these three parameters and adjusting the weights to maximize the fraction of lines=B sources in the cohort of sources with the lowest scores. Because of the relatively small size of the lines=B sample, continuous optimization algorithms such as Newton's minimization method could not be used. Instead, this optimization was done iteratively by hand. This yielded the following figure of merit parameterization (only 2 of the 3 weights are independent) of the infrared colors, denoted S_I:

$$S_I = 1.7\ c_2 + 2.0\ c_3 + c_4.$$

Sources with infrared colors close to the AGN template have a low score, while those with large differences are scored high. This is seen in the first column of Figure 2, which shows a modest separation: most sources with $S_I < 0.888$ were non-AGN while most with $S_I > 0.888$ tend to be AGN. The larger weights for the 'color cut-off' functions c2 and c3 are needed, since those colors span a shorter wavelength baseline than does c4.

2.5. Constructing the RASS distance discriminator

Next we construct a second parameter S_X, based on the WISE-RASS source distance:

$$S_X = (d/e)^2,$$

where d is the distance from the WISE source to the nearest RASS source and e is the uncertainty in d (both in arcseconds). A typical RASS source positional uncertainty is e=15. The ratio is a good indicator of the likelihood that the WISE source has an associated RASS source. The logarithm of this parameter is shown in the second column of Figure 2, which again shows good separation: a large fraction of sources with $\log_{10}(S_X) < 0.969$ were non-AGN while most with $\log_{10}(S_X) > 0.969$ were AGN. The sense of this parameter is the same as before: a smaller value indicates a higher likelihood of an associated X-ray source (and therefore that the source is an AGN), and it is positive-definite.

2.6. Synthesizing the final statistic

Because these parameters were derived independently (one based on infrared color, and the other on the distance to the nearest X-ray source), combining them should provide even sharper classification. Again, we made a linear combination with relative weighting by hand, to maximize the fraction of lines=B objects. The logarithm is then taken to collapse the values to a more manageable range. This yielded a combined statistic:

$$S_{IX} = \log_{10}(S_I + 0.116\ S_X),$$

This is shown in the third column of Figure 2. Note the very strong separation in the bottom diagram: of the 329 SDSS sources with $S_{IX} < 0$, 309 (94%) had lines=B, indicating an initial Type I error rate of ~6%.

3. Spectroscopic testing

3.1. Construction of the bright object test sample

The sources SDSS chose to observe were not drawn randomly from the larger population, as can be seen by the differences in the first two rows of Figures 1 and 2. For instance, note that relative to the SDSS sample, the full sample shows an excess of sources with H-K > 0.8 and/or W1-W2 > 0.5. This means that more field sources have favorable H-K and/or W1-W2 colors than the SDSS subsample, so it is necessary to make an independent test of the Type I error rate.

In order to test the error rate, it is it necessary to examine a fair (random) sample of the full sample, rather than those that SDSS selected for spectroscopy. Accordingly, we identified a subsample of the brightest northern W2R sources in the winter sky. Table 2 lists the 77 sources with $S_{IX} < 0$, J < 14.0, R.A. between 21^h and 15^h, and Dec. > -20^o, sorted so that sources with the lowest (most favorable) value of S_{IX} are at the top. Of these, 70 (91%) were listed in VCV: 69 have VCV classifications consistent with our AGN definition: S1-S1.9 (57), BL (5), HP (4), Q (2), AG (1). One (UGC 7252) is classified as S2, this does not fit our limited definition of an AGN. Finally, 7 of the W2R sources meeting the above criteria were not listed in VCV.

3.2. Spectroscopy with the Lick Observatory 3-m Telescope

In order to complete identifications of this sample, we observed these seven remaining sources on December 19 and 20, 2011 with the Kast double spectrograph on the Shane 3-m reflector. The blue channel covered wavelengths from the atmospheric cutoff to the dichroic cutoff at 5500 Å; the red channel covered from 5600 to 8200 Å. The slit width was 3"; the spectrum was extracted over a length of 5" to 7". Typical exposure times were 600 to 1200 seconds. Reductions to one-dimensional spectra, including bias-subtraction, flat-fielding and sky subtraction, were done using standard procedures in the twodspec apall packages of IRAF. Flux calibration, made by comparison with standard stars observed during twilight, is generally accurate to about 20%.

These spectra are presented in Figure 3, again sorted by S_{IX}. We find that all seven are AGN: six Seyfert 1s/quasars and one BL Lac object (W2R 0814-10). We also confirmed the VCV identification of UGC 3752 as a Seyfert 2. With these data, the entire bright AGN test sample has been fully identified. This indicates that all but one of the 77 sources with $S_{IX} < 0$ are AGN, indicating a formal Type I error rate of 1/77=1.4%. Note, however, that because the error on unity is unity, and it would be more accurate to conservatively quote a Type I error rate of $\lesssim$5%, corresponding to a success rate of $\gtrsim$95%.

3.3. Extrema of S_X and S_I

A cutoff at $S_{IX} < 0$ implies that $\log_{10}(S_I + 0.116S_X) < 0$ and thus $S_I + 0.116S_X < 1$. Since both S_I and S_X are positive definite, this means that both S_I and $0.116S_X$, must each be less than 1. Each of these has a simple, convenient interpretation. First, since $S_X = (d/e)^2$, this implies $d < 0.116^{-1/2}\, e$, or $d < 2.9\, e$. That is, the infrared source must have an X-ray source within ~3σ or it cannot be included in the W2R sample irrespective of its infrared colors.

Second, the limit $S_I < 1$ means that the source must have "AGN-like" infrared colors. As discussed above, AGN show a characteristic power-law continuum between 2 and 12μm. This AGN component fills in the "valley" in the SED that is otherwise left between the coolest red giants (whose emission peaks at 1.6 μm) and the warmest dust grains (which emit strongly in the PAH emission bands around 8–11 μm, due to non-thermal spiking in very small grains). The AGN infrared component has been described as thermal re-radiation of the continuum from the central engine by hot dust grains outside the BLR (e.g., Pott et al. 2010). However, it is also

well-known that a nonthermal synchrotron component produces a very similar power-law spectral shape (e.g. Edelson & Malkan 1986). Regardless of what its physical origin may be, this power-law mid-infrared continuum appears to be present in virtually every galactic nucleus which also has clearly detectable broad emission lines. It is also seen in some galaxies which are classified as Seyfert 2s, or even LINERs, probably because they too have a broad-line region (BLR), which is obscured from direct view. Since the extinction is less than a tenth of that in the optical, the method should work even in heavily dust-obscured galactic nuclei, even where optical methods could fail. However these obscured AGN will tend not to be detected in the X-rays, so they do not generally make it into this sample.

Starburst galaxies (i.e., lacking a true nonstellar AGN) have some hot dust which may be detectable at 3 μm, or even 2 μm, but it produces relatively much weaker continuum than the cooler dust. Therefore, very few starbursts have the mid-infrared power-law continua characteristic of AGN. On the other hand, nearly all AGN have it, so long as the strength of the AGN, relative to the underlying starlight of the host galaxy, is high enough.

Although some blazars probably lack a BLR, and may also lack this "hot" AGN component in the near-to-mid IR, they nonetheless have another, non-thermal, infrared power-law, which is known (from its high polarization and violent variability) to be direct synchrotron emission from a relativistically-beamed jet. Thus it is a fortunate coincidence that our same IR-color method is effective at picking out special galactic nuclei with either Seyfert 1 or blazar components.

4. Applications of the S_{IX} statistic to AGN Searches

4.1. Derivation of the W2R sample

The S_{IX} statistic was optimized and tested with preliminary WISE data covering ~57% of the sky. The final WISE data release on 13 March 2012 made it possible to apply this technique to the full sky with superior data. Accordingly, we applied the SQL command "w1mpro >= 9 and w1snr >= 10 and w2snr >= 10 and w3snr >= 10 and w4snr >=10 and n_2mass = 1 and j_msig_2mass <= 0.10866 and h_msig_2mass <= 0.10866 and k_msig_2mass <= 0.10866" to the WISE All-Sky Catalog at http://irsa.ipac.caltech.edu/cgi-bin/Gator/nph-scan to yield a sample of 884,556 sources. Note that this formulation differs slightly from that in Section 2.1., but these small improvements should not make any significant difference.

The main difference between the preliminary and final WISE data releases is that the latter catalog determines fluxes from "second pass" rather than "first pass" PSF-fitting. For the typical (i.e., faint) sources near the limits of our SNR cuts, the second pass PSF fit gives more accurate fluxes (see Figure 7 in http://wise2.ipac.caltech.edu/docs/release/allsky/expsup/sec6_3c.html). In the W1 band, the new fluxes are typically about 10% lower. The resulting colors are hardly changed from those given in the Preliminary release, but the SNR=10 limit has now become slightly more restrictive than before.

This application resulted in a sample of 4,316 sources with $S_{IX} < 0$. Table 3 lists these sources, referred to as the W2R AGN sample, for WISE/2MASS/RASS. By comparison, the preliminary WISE database yielded only 1,924 sources with $S_{IX} < 0$, so use of the final data release produced an improvement of a factor of ~2.2 in sample size.

The SQL command restricts the WISE sample to objects fainter than W1 = 9 in order to screen out a large number of stars. This was necessary both to facilitate data management as well as to minimize contamination from stars when searching for AGN in the Galactic plane.

This criterion however also eliminates a few dozen very bright AGN. The brightest AGN in the W2R sample is NGC 5548, which has W1 = 9.16. For comparison NGC 4151, the brightest AGN in the sky at many wavelengths has W1 = 6.90. For a roughly Euclidean flux/count relation, this difference of 2.26 magnitudes corresponds to ~23 missed sources. Thus the absence of some famous, very bright AGN, e.g., 3C 273 and all of the original Seyfert (1943) galaxies except NGC 5548 should not be taken as an error in our procedures. As discussed in the conclusions, we plan to investigate relaxing this cutoff in future work.

4.2. "Completeness" of the VCV catalog

We used the VCV spectroscopic galaxy classification to organize these sources into four subclasses: Seyfert 1 AGN (VCV classifications "S," "S1-S1.9," "Q," and "AG"), blazar AGN (VCV classifications "BL" and "HP"), non-AGN, and unclassified (not in the VCV catalog). (By our restricted definition, VCV classification "S2," and "S3", which includes LINERs and even some starbursts, all count as non-AGN). Only 2,209 of the 4,316 sources in the full list (51%) were in VCV at the time of this experiment. However, of the 77 sources in AGN test sample (those with J < 14 in a region of the northern sky), 70 (91%) are classified as AGN in VCV. Thus even though the VCV catalog was never intended to be a complete catalog of AGN, it nonetheless provides a very good census of bright (J < 14) AGN. It is less than half as complete for sources ~2 magnitudes fainter. It also reflects the much greater completeness of AGN searches in the northern hemisphere due to more extensive spectroscopic capabilities of ground-based telescopes there over the last several decades.

Further, we note that the sample of 2,209 identified sources breaks down into 2,104 Seyfert 1s, 87 blazars, and 18 non-AGN. Thus Seyfert 1s make up 2,104/(2,104+87) ~ 96% of the identified AGN sample and blazars make up the other ~4%. The formal Type I error rate is again small, 18/2,104 ~ 1%. But this is also a highly uncertain estimate, this time because an unknown bias may cause a different fraction of the 49% of unidentified sources to be non-AGN.

In order to test the completeness of the VCV catalog to AGN, Figure 5 shows the relative sizes of each of these four subsamples as a function of source brightness, declination and galactic latitude. Note that the completeness of the VCV catalog decreases strongly to fainter J magnitudes. Completeness also decreases to lower (more southern) declinations, with a fairly strong transition near the celestial equator. There is a hint of an increase in incompleteness at very northern declinations as well, but this is only seen in one data point. Finally there is also a clear increase in incompleteness near the galactic plane (small values of absolute magnitude of galactic latitude, |b|).

4.3. New Kepler AGN

One early motivation for this study was to identify AGN that could be observed with Kepler, as that satellite is producing light curves with precision and sampling that are more than an order of magnitude better than the best obtainable from the ground (see Mushotzky et al. 2011 for details). That satellite requires sources to be previously identified before their data can be downloaded, but because the field lies near the galactic plane, only two bright AGN (Zw 229-15 and 1RXS J192949.7+462231, both Seyfert 1 galaxies) were known at the start of that mission. Our group utilized the methods of Stocke et al. (1983), Malkan (2004), and an earlier incarnation of the S_{IX} technique to identify and begin to monitor an additional 13 AGN in the Kepler field.

These now have spectroscopic confirmations from the Kast double spectrograph on the Lick 3-m telescope. The observations, obtained in July 2011 were reduced in the same way as

described above for the December 2011 run, except that the slit width was 2.0", affording slightly better spectral resolution. These spectra are shown in Figure 6, and source details are given in Table 4. Note that the first 10 of the confirmed AGN in Table 4 are members of the W2R sample, the next (W2 1925+50) fell slightly outside the $S_{IX} < 0$ cutoff, and the last two are not in either sample. Note also that W2R 1926+42 is a BL Lac object.

5. Conclusions

It has long been known that AGN have distinctive properties in both the X-rays and infrared. This paper combines available data from three all-sky surveys – WISE, 2MASS and RASS – in order to develop the "S_{IX}" statistic that can identify AGN with high ($\gtrsim$95%) confidence. The method was optimized with preliminary WISE data and SDSS-8 spectra and independently tested with the Lick 3-m Kast spectrograph. It was then applied to the final WISE data release to produce the "W2R" AGN sample contains nearly 2,000 new, bright ($J \lesssim 16$) AGN.

While neither this sample nor the VCV catalog claims to be "complete," it is possible to use each to test and quantify the biases and incompleteness in the other. We find that the VCV catalog presents a good census (~90% completeness) for northern (declination > -20^o), bright ($J < 14.0$) sources, but the completeness falls below 50% for southern, fainter sources.

The success of this approach also indicates that "classic" AGN – Seyfert 1s, quasars and blazars – share two common properties. First, they tend to be strong soft X-ray sources. Second, their infrared SEDs are strongly dominated by a smooth, relatively flat power-law. This distinguishes them from so-called "obscured AGN" – Seyfert 2s, LINERs, ULIRGs, etc. – that have steep and bumpy infrared SEDs and are generally not detected in the soft X-rays.

Finally, we hope to make further improvements on this technique in the future. For instance the S_{IX} statistic was derived using WISE preliminary data but applied to the WISE final data release. We plan to re-derive it using the final dataset and then confirm the results with spectroscopy at Lick over the next year. We will investigate relaxing the $W1 > 9$ brightness cutoff in order to increase the number of very bright AGN. We will also utilize Lick spectroscopy to confirm new AGN candidates from the final survey in the Kepler field. Finally we will examine the much larger and less reliable W2 sample, given in the appendix below.

Acknowledgements

The authors would like to thank Richard Mushotzky and Wayne Baumgartner for insights into using X-ray data to identify AGN, and Tom McGlynn for help with the HEASARC program Xamin. We also thank the anonymous referee and Joan Wrobel, the Astrophysical Journal Scientific Editor, for a timely and helpful review of this paper. This research has made extensive use of data obtained from the High Energy Astrophysics Science Archive Research Center (HEASARC), provided by NASA's Goddard Space Flight Center, the NASA/IPAC Infrared Science Archive (IRSA), operated by the Jet Propulsion Laboratory, California Institute of Technology, under contract with NASA, and the Sloan Digital Sky Survey (please see http://www.sdss.org/collaboration/credits.html for details).

Appendix: The W2 (WISE/2MASS) sample

Here we modify of our analysis to derive a sample with a good Type II error rate instead of the main focus of the paper, which is to derive a sample with a good Type I error rate. That is,

the method and sample presented in this section is focused on identifying almost all of the lines=B sources, at the expense of a relatively large number of false positives.

There are two main differences between the two statistics and samples. The first is that RASS data are not used in this analysis, because only 410 of the 741 SDSS lines=B sources (~56%) show a RASS source within 3σ of the infrared position. (While it appears that all or almost all AGN can be detected with sufficiently long exposures, the typical ~350 sec RASS integrations were just not long enough to detect all sources.) Thus only S_I is used in this analysis. The second difference is that a more liberal cutoff was used because the goal is to minimize the Type II errors. We drew a cutoff at $S_I < 1.73$.

Of the 741 SDSS objects with lines=B, 701 (95%) have $S_I < 1.73$, corresponding to a Type II error rate of ~5%. There are 1,255 SDSS sources with $S_I < 1.73$, indicating a success rate of 701/1,255 = 56% (at best). Of the full sample of 884,556 sources, 55,050 (6.2%) have $S_I < 1.73$. This is referred to as the W2 (for WISE/2MASS) sample. Its value is that it comes closer than the W2R sample to producing a complete sample of the AGN population, albeit at the cost of a far larger, and ill-determined Type I error rate.

Of these 55,050 sources, 4,774 have VCV identifications as AGN. This yields a lower limit on the success rate of 4,774/55,050 = 9%. Thus the Type I error rate is currently rather poorly-constrained to the range 44-91%. We plan to obtain Lick 3-m spectroscopy in the coming year in order to directly determine the W2 Type I error rate. Finally note that 543 of the W2 sources have VCV identifications of S2/S3, suggesting that 542/(4,774+543) = 10% of the identified W2 sample are narrow-line objects. This is much larger than the 0.5% of narrow-line sources in the identified W2R sample, confirming that the presence of a nearby RASS source selects against narrow emission line galaxies.

References

Assef, R. et al 2010 ApJ 713, 970
Borucki, W. et al. 2010, Science, 327, 977
Edelson, R., Malkan, M. 1986, ApJ, 308, 59
Edge, D. et al. 1959, Mem.RAS. 68, 37
Fisher, R. A., *The Design of Experiments*, Oliver & Boyd (Edinburgh), 1935
Green, R., Schmidt, M., Leibert, J. 1986, ApJS, 61, 305
Hasinger, G., Lehmann, I., Giacconi, R., et al. 1999, Highlights in X-ray Astronomy
Lacy, M. et al 2004, ApJS 164, 156
Malkan, M. 2004, ASPC, 311, 449.
Malkan, M. A., Moore, R. L. 1986, ApJ, 300, 216
Malkan, M. A., Sargent, W. L. 1982, ApJ, 254, 282
Markarian et al. 1989, SoSAO, 62, 5
Marshall, H. L.; Tananbaum, H.; Huchra, J. P.; Zamorani, G.; Braccesi, A.; Zitelli, V. 1983, ApJ, 269, 42
Mushotzky, R. et al. 2011, ApJL, 743, L12
Pott, J. et al. 2010, ApJ, 715, 736
Rush, B., Malkan, M. A. 1996, ApJ, 456, 466
Rush, B., Malkan, M. A., Fink, H. H., Voges, W. 1996, ApJ, 471, 190
Seyfert, C. 1943, ApJ, 97, 28
Skrutskie, M. et al. 2006, AJ, 131, 1163
Stern, D. et al. 2005, ApJ, 631, 163

Stocke, J. et al. 1983, ApJ, 273, 458.
Sun, W. H., Malkan, M. A. 1989, ApJ, 346, 68
Veron-Cetty M.-P., Veron, P. 2006, A&A, 445, 773 (VCV)
Voges, W. et al. 1999, A&A, 348, 38
Wright, E. et al. 2010, AJ, 140, 1868
York, D. et al. 2000 AJ, 120, 1579

Table 1: Mean colors and parameters for the three input samples

Color/	Full			SDSS			lines=B			
Parameter	Mean	Median	S.D.	Mean	Median	S.D.	Mean	Median	S.D.	Contrast
J-H	0.94	0.82	0.48	0.75	0.75	0.13	0.77	0.78	0.17	0.20
H-K	0.54	0.50	0.30	0.53	0.50	0.19	0.77	0.78	0.22	1.34
W1-W2	0.37	0.28	0.37	0.43	0.32	0.32	0.91	0.94	0.25	2.17
W2-W3	3.01	3.20	1.16	3.61	3.72	0.55	2.93	2.90	0.35	1.82
W3-W4	2.34	2.28	0.71	2.24	2.24	0.39	2.33	2.32	0.25	0.25
S_I	2.57	2.64	1.22	2.21	2.52	0.96	0.62	0.45	0.58	2.71
$\log_{10}(S_X)$	3.30	3.44	0.96	2.74	3.10	1.10	1.30	0.51	1.75	1.82
S_{IX}	2.41	2.51	0.83	1.91	2.17	0.86	0.83	0.17	1.32	1.84

Table notes: The first column gives the measured color (for the first five rows) or parameterization (for the last three). The next nine columns give the mean, median and standard deviation for each color (or parameter), for the full WISE/2MASS/RASS sample, the SDSS subsample, and the lines=B subsample, respectively. The last column gives the "contrast" between the SDSS and lines=B samples; that is, the absolute value of the difference between the samples' median color (or parameter) divided by the mean standard deviation. Note that the colors J-H and W3-W4 show a relatively small contrast, but the other three colors show a large contrast. This makes those colors, H-K, W1-W2 and W2-W3 better-suited for distinguishing AGN from other objects in the Sloan survey.

Table 2: Bright AGN test sample

Row	Source Name	RA	Dec	J	S_{IX}	S_I	$\log_{10}(S_X)$	Type	z	2MASS ID	RASS (1RXS J...)
1	3C 120	04 33 11.08	+05 21 15.6	12.67	-1.319	0.019	-0.602	S1.5	0.033	776090812	043311.2+052112
2	MARK 9	07 36 57.01	+58 46 13.5	13.08	-1.212	0.045	-0.852	S1.5	0.039	1057769027	073657.0+584610
3	IRAS F07144+441	07 18 00.60	+44 05 27.2	13.32	-1.129	0.072	-1.688	S1.5	0.061	585728155	071800.7+440527
4	IRAS 04416+1215	04 44 28.77	+12 21 11.7	13.93	-1.097	0.067	-0.954	S1n	0.089	1283847063	044428.6+122113
5	NPM1G-05.0216	04 47 20.71	-05 08 14.0	13.63	-1.003	0.064	-0.510	S1.5	0.044	197517295	044720.4-050813
6	MARK 1383	14 29 06.59	+01 17 06.1	13.04	-0.957	0.094	-0.852	S1.0	0.086	1259029691	142906.7+011708
7	MARK 79	07 42 32.81	+49 48 35.0	12.55	-0.899	0.067	-0.292	S1.2	0.022	880738049	074232.9+494830
8	NPM1G-14.0512	13 41 12.89	-14 38 40.1	13.24	-0.893	0.039	-0.116	S1n	0.042	1253848597	134112.5-143836
9	SNU J04255+3447	04 25 33.10	+34 47 19.5	13.63	-0.866	0.107	-0.602	S1	0.058	1311860102	042533.0+344715
10	RXS J04520+4932	04 52 04.76	+49 32 44.8	13.09	-0.824	0.112	-0.486	S1	0.029	813145631	045205.0+493248
11	MCG -02.14.009	05 16 21.21	-10 33 41.3	13.19	-0.745	0.151	-0.602	S1	0.028	115706031	051621.5-103341
12	RXS J03370+4738	03 37 02.91	+47 38 50.2	13.57	-0.692	0.087	0.000	S1	0.184	421944963	033703.9+473852
13	UM 614	13 49 52.85	+02 04 45.2	13.67	-0.670	0.208	-1.306	S1.8	0.033	866975302	134952.7+020446
14	PG 0844+349	08 47 42.44	+34 45 04.6	13.41	-0.658	0.213	-1.203	S1.0	0.064	190208819	084742.5+344506
15	B2 0321+33	03 24 41.15	+34 10 46.0	13.93	-0.640	0.113	0.000	S1n	0.063	174522289	032441.3+341056
16	PG 1448+273	14 51 08.78	+27 09 26.9	13.64	-0.622	0.123	0.000	S1n	0.065	694625518	145108.5+270933
17	RXS J06021+2828	06 02 10.46	+28 28 19.4	12.23	-0.609	0.208	-0.486	S1	0.033	149712032	060210.7+282821
18	**W2R 0502+22**	**05 02 58.22**	**+22 59 51.8**	**13.23**	**-0.600**	**0.228**	**-0.704**	**S1**	**0.057**	**144694350**	**050258.5+225949**
19	HS 0306+1051	03 08 56.70	+11 03 15.4	13.62	-0.584	0.103	0.134	Q	0.150	846330760	030855.8+110320
20	HS 0710+3825	07 13 40.27	+38 20 39.9	13.35	-0.571	0.180	-0.116	S1n	0.123	850552011	071339.7+382043
21	RXS J04344+7127	04 34 29.11	+71 28 02.0	13.80	-0.551	0.236	-0.408	S1.5	0.025	909346139	043429.0+712757
22	MARK 124	09 48 42.68	+50 29 31.5	13.85	-0.543	0.201	-0.134	S1n0	0.056	972705125	094841.6+502926
23	NGC 985	02 34 37.81	-08 47 15.9	12.74	-0.543	0.265	-0.736	S1.5	0.043	103425681	023438.0-084714
24	PKS 0422+00	04 24 46.83	+00 36 06.3	12.90	-0.532	0.254	-0.468	HP		773008941	042446.8+003559
25	S5 0716+71	07 21 53.44	+71 20 36.2	11.94	-0.527	0.252	-0.408	BL		575064129	072153.2+712031
26	SNU J03569+4255	03 56 57.01	+42 55 40.5	13.54	-0.434	0.326	-0.444	S1	0.066	814116054	035657.3+425536
27	IRAS 03450+0055	03 47 40.18	+01 05 14.0	12.99	-0.421	0.019	0.492	S1.5	0.031	778498712	034738.7+010543
28	MARK 1044	02 30 05.51	-08 59 53.1	12.46	-0.393	0.397	-1.203	S1n	0.017	103338235	023005.5-085951
29	MARK 813	14 27 25.05	+19 49 52.4	13.86	-0.385	0.374	-0.486	S1.0	0.111	1099804429	142725.3+194954
30	B3 0754+394	07 58 00.04	+39 20 29.0	12.91	-0.372	0.381	-0.422	S1.5	0.096	850696538	075759.7+392036
31	S5 2116+81	21 14 01.14	+82 04 48.2	13.83	-0.365	0.410	-0.736	S1.0	0.086	902844140	211400.0+820447
32	MCG -02.12.050	04 38 14.18	-10 47 44.9	13.73	-0.365	0.398	-0.538	S1.0	0.036	136924508	043813.8-104740
33	MS 04124-0802	04 14 52.65	-07 55 39.6	12.73	-0.363	0.194	0.315	S1.5	0.037	144094444	041451.8-075521
34	IRAS 06269-0543	06 29 24.76	-05 45 26.4	13.41	-0.327	0.290	0.194	S1n	0.117	129481404	062925.1-054535
35	HS 1046+8027	10 50 35.67	+80 11 50.7	13.71	-0.310	0.134	0.486	S1	0.115	852452906	105037.1+801204

Table notes: Sources that meet the following criteria: detected at >10σ in all WISE and 2MASS bands, $S_{IX} < 0$, J < 14, Right Ascension between 21^h and 15^h, and Declination > -20^o. Of the 77 sources in this list, 70 are also listed in the VCV catalog. The remaining 7 sources were observed with the Lick 3-m; they are shown in boldface. The source name (taken from VCV when possible, otherwise denoted by a positional name) is given in the first column, followed by Right Ascension and Declination (taken from the WISE catalog) in Columns 2 and 3. The source identifications and redshifts (taken from VCV when available, otherwise derived from the spectra presented in Figure 3) are given in Columns 4 and 5. Newly-identified sources are shown in boldface and sources that do not meet our AGN criteria are shown in italics. The measured values of J are given in Column 6, and the parameterizations S_I, $\log_{10}(S_X)$ and S_{IX} are given in Columns 7-9. The 2MASS identifier and RASS source name are given in Columns 10 and 11. Table is sorted in ascending order in S_{IX}.

Table 2: Bright AGN test sample (continued)

Row	Source Name	RA	Dec	J	S_{IX}	S_I	$\log_{10}(S_X)$	Type	z	2MASS ID	RASS (1RXS J...)
36	MARK 110	09 25 12.85	+52 17 10.5	13.87	-0.310	0.284	0.250	S1n	0.035	783924768	092512.3+521716
37	MARK 618	04 36 22.28	-10 22 33.9	13.20	-0.308	0.340	0.116	S1.0	0.035	136884757	043622.3-102226
38	1WGA J0310+405	03 10 06.23	+40 56 54.3	13.51	-0.297	0.470	-0.526	BL	0.137	380812710	031006.2+405700
39	PKS 0829+046	08 31 48.88	+04 29 39.1	13.04	-0.290	0.260	0.338	HP	0.180	804079605	083147.7+043005
40	VII Zw 118	07 07 13.09	+64 35 59.0	13.67	-0.265	0.522	-0.736	S1.0	0.079	535071464	070713.5+643558
41	UGC 3478	06 32 47.16	+63 40 25.4	12.94	-0.260	0.485	-0.250	S1n	0.012	518331815	063248.0+634026
42	SNU J05547+6620	05 54 47.24	+66 20 43.9	13.67	-0.249	0.397	0.158	S1	0.186	543721984	055448.8+662036
43	PKS 0405-12	04 07 48.42	-12 11 36.6	13.76	-0.244	0.524	-0.408	S1.2	0.574	729336554	040748.7-121133
44	**W2R 0535+40**	**05 35 32.12**	**+40 11 15.8**	**13.86**	**-0.243**	**0.526**	**-0.408**	**S1**	**0.019**	**459530968**	**053532.6+401116**
45	Z 0214+083	02 17 17.11	+08 37 04.0	13.83	-0.216	0.410	0.233	BL	1.400	1133315111	021716.0+083707
46	PG 0804+761	08 10 58.63	+76 02 42.5	12.98	-0.210	0.595	-0.736	S1.0	0.100	1295367017	081059.0+760245
47	MG J0509+0541	05 09 25.96	+05 41 35.3	12.71	-0.206	0.431	0.218	BL		780403237	050927.0+054145
48	RXS J06080+3058	06 08 00.80	+30 58 41.5	14.00	-0.205	0.487	0.070	S1	0.073	874128285	060801.7+305847
49	2E 0507+1626	05 10 45.53	+16 29 58.1	13.39	-0.194	0.581	-0.292	S1.5	0.017	1217738633	051045.4+162953
50	**W2R 0413+72**	**04 13 37.62**	**+72 06 52.5**	**13.67**	**-0.179**	**0.647**	**-0.878**	**S1**	**0.105**	**547701979**	**041337.5+720649**
51	HS 0624+6907	06 30 02.51	+69 05 03.9	13.25	-0.179	0.574	-0.116	Q	0.370	763053340	063001.7+690458
52	Ton 1015	09 10 37.04	+33 29 24.6	13.98	-0.176	0.638	-0.602	BL	0.354	205603292	091037.2+332920
53	MARK 205	12 21 44.10	+75 18 38.3	13.60	-0.167	0.444	0.310	S1.0	0.070	583065747	122144.4+751848
54	MARK 374	06 59 38.09	+54 11 47.6	13.51	-0.163	0.425	0.352	S1.2	0.044	504498144	065938.5+541136
55	MARK 141	10 19 12.55	+63 58 02.7	13.62	-0.163	0.670	-0.852	S1.2	0.042	911287970	101912.1+635802
56	MARK 10	07 47 29.06	+60 56 00.8	13.34	-0.162	0.680	-1.088	S1.0	0.030	760619126	074729.4+605601
57	**W2R 0406+11**	**04 06 22.05**	**+11 52 15.6**	**13.94**	**-0.158**	**0.531**	**0.149**	**S1**	**0.033**	**1310414811**	**040621.6+115233**
58	*UGC 3752*	*07 14 03.84*	*+35 16 45.4*	*12.44*	*-0.126*	*0.524*	*0.285*	*S2*	*0.016*	*1230840575*	*071404.6+351622*
59	RX J03140+2445	03 14 02.72	+24 44 32.8	13.82	-0.123	0.290	0.602	AG	0.054	123793901	031401.2+244504
60	**W2R 0228+28**	**02 28 55.33**	**+28 09 04.5**	**13.95**	**-0.122**	**0.615**	**0.083**	**S1**	**0.036**	**350481074**	**022857.8+280904**
61	RXS J05524+5928	05 52 28.15	+59 28 37.0	12.53	-0.120	0.553	0.250	S1	0.058	723962675	055229.5+592842
62	MARK 595	02 41 34.86	+07 11 13.8	12.98	-0.107	0.730	-0.352	S1.5	0.028	1155145092	024135.2+071117
63	MARK 684	14 31 04.79	+28 17 14.1	13.22	-0.096	0.795	-1.203	S1n	0.046	586673408	143104.8+281716
64	NGC 1019	02 38 27.40	+01 54 27.8	13.67	-0.092	0.804	-1.306	S1.5	0.024	1098807494	023827.5+015426
65	**W2R 0157+47**	**01 57 10.94**	**+47 15 59.2**	**13.67**	**-0.088**	**0.765**	**-0.352**	**S1**	**0.047**	**459180062**	**015711.8+471607**
66	NPM1G-16.0109	02 56 02.62	-16 29 15.4	13.65	-0.081	0.796	-0.538	S1.9	0.032	40931691	025601.7-162919
67	IRAS 04312+4008	04 34 41.53	+40 14 21.5	12.97	-0.058	0.759	0.000	S1n	0.020	369140072	043442.1+401425
68	3C 66A	02 22 39.60	+43 02 07.8	12.64	-0.053	0.844	-0.457	HP		1316752374	022239.1+430220
69	1ES 0206+522	02 09 37.40	+52 26 39.5	13.97	-0.041	0.758	0.116	S1	0.049	476576303	020936.8+522645
70	**W2R 0814-10**	**08 14 11.69**	**-10 12 10.2**	**13.41**	**-0.039**	**0.819**	**-0.083**	**BL**		**213426127**	**081411.7-101200**
71	PKS 1424+240	14 27 00.40	+23 48 00.1	12.68	-0.038	0.900	-0.852	HP		1099812234	142700.5+234803
72	NPM1G+78.0048	12 42 36.13	+78 07 20.4	13.75	-0.035	0.511	0.550	S1.9	0.022	987868938	124250.9+780738
73	UGC 3901	07 33 53.11	+49 17 31.0	13.98	-0.027	0.883	-0.310	S1.9	0.022	972501261	073353.4+491737
74	IRAS 04576+0912	05 00 20.76	+09 16 55.7	13.85	-0.025	0.517	0.565	S1n	0.037	968100516	050022.3+091659
75	UGC 6728	11 45 15.95	+79 40 53.4	13.10	-0.025	0.941	-1.688	S1.2	0.006	846701200	114516.1+794054
76	NPM1G-03.0212	04 46 56.74	-03 05 11.7	13.62	-0.021	0.952	-1.803	S1	0.031	197501982	044656.8-030513
77	RXS J03000+1630	03 00 07.99	+16 30 14.5	13.76	-0.002	0.708	0.393	S1	0.035	800837315	030007.6+163023

Table 3: W2R sample

Row	2MASS ID	RA	Dec	J	S_{IX}	S_I	$\log_{10}(S_X)$	RASS Name	VCV Name	Type	z
1	4356519	12 46 46.81	-25 47 49.1	14.384	-2.309	0.004	-2.108	1RXS J124646.7-254749	PKS 1244-255	HP	0.638
2	977486214	07 53 01.38	+53 52 59.8	15.467	-2.016	0.003	-1.243	1RXS J075301.1+535305	S4 0749+54	BL	0.2
3	145276761	07 38 07.02	+21 27 29.6	15.343	-1.986	0.000	-1.051	1RXS J073806.9+212726			
4	249700394	12 25 27.18	-04 18 57.1	14.738	-1.913	0.008	-1.438	1RXS J122527.1-041857	RXS J12254-0418	S1	0.137
5	762994872	03 05 36.50	+76 22 56.2	15.268	-1.891	0.008	-1.380	1RXS J030536.7+762257			
6	740172497	07 03 24.24	-60 15 22.5	13.294	-1.885	0.011	-1.757	1RXS J070324.1-601525			
7	617850898	22 48 41.16	-51 09 53.1	14.565	-1.841	0.000	-0.906	1RXS J224841.4-510951	2RE J2248-510	S1.5	0.102
8	169461995	02 38 45.14	-30 48 23.3	13.530	-1.838	0.005	-1.086	1RXS J023845.4-304825	ESO 416-G05	S1.2	0.063
9	618425984	05 02 52.38	-47 13 30.5	15.782	-1.814	0.000	-0.879	1RXS J050252.6-471326			
10	995435651	04 08 40.54	+30 39 12.4	15.601	-1.761	0.017	-2.549	1RXS J040840.5+303912			

Table notes: Sources in the W2R sample of highly-likely AGN candidates. Table 3 is published in its entirety in the electronic edition of the Astrophysical Journal, and can also be downloaded from http://www.astro.ucla.edu/~malkan/w2r/table3.xls. A portion is shown here for guidance regarding its form and content. The 2MASS identifier is given in the first column, followed by Right Ascension and Declination in Columns 2 and 3. The measured values of J are given in Column 4, and the parameterizations S_I, $\log_{10}(S_X)$ and S_{IX} are given in Columns 5-7. The RASS source name is given in Columns 8. If a source is listed in the VCV catalog, the source name, redshift and identification from that catalog are given in Columns 9-11. Previously unidentified are shown in boldface while those that do not fit this paper's definition of AGN are shown in italics.

Table 4: Lick spectroscopy of Kepler field AGN

ID	RA	Dec	J	S_{IX}	z	Kepler ID	Comments
W2R 1914+42	19 14 15.50	+42 04 59.9	15.71	-0.603	0.502	6595745	Hβ,OIII
W2R 1920+38	19 20 47.75	+38 26 41.3	16.04	-0.382	0.368	3337670	Hβ,OIII,MgII
W2R 1931+43	19 31 12.56	+43 13 27.6	15.49	-0.326	0.439	7610713	Hα/N2
W2R 1858+48	18 58 01.11	+48 50 23.4	15.87	-0.323	0.079	11178007	Hα,Hβ,Hg
W2R 1904+37	19 04 58.65	+37 55 41.0	14.34	-0.309	0.089	2694185	Hα/N2
W2R 1910+38	19 10 02.50	+38 00 09.6	15.76	-0.275	0.130	2837332	Hα/N2
W2R 1853+40	18 53 19.28	+40 53 36.4	15.24	-0.219	0.625	5597763	MgII,Hβ
W2R 1845+48	18 45 59.57	+48 16 47.6	15.43	-0.167	0.152	10841941	Hα,NaD,HK
W2R 1931+38	19 31 15.49	+38 28 17.2	16.02	-0.136	0.158	3347632	Hα/N2
W2R 1926+42	19 26 31.05	+42 09 59.0	15.59	-0.076	0.154	6690887	BL Lac NaD,HK
W2 1925+50	19 25 02.18	+50 43 13.8	14.23	0.218	0.067	12158940	Hα/N2
1915+41	19 15 09.13	+41 02 39.1	15.69		0.220	5781475	Hα,OIII
1922+45	19 22 11.23	+45 38 06.2	15.92		0.115	9215110	Seyfert 1.9 Hα/N2

Table notes: New AGN in the Kepler field. The last column gives the strongest spectral features identified in each spectrum, which were used to derive the redshift. In nearly all cases they are emission lines (except for the stellar absorption lines found in the one BL Lac object. The first 10 sources are in the W2R sample; they are sorted by S. The next fell slightly outside the cutoff but is in the W2 sample. The last two were not included in either sample; they were initially found by the techniques of Stocke et al. (1983) and Malkan (2004).

Table 5: W2 sample

Row	2MASS ID	RA	Dec.	J	S_I	VCV Name	Type	z
1	617850898	22 48 41.16	-51 09 53.1	14.565	0.000	2RE J2248-510	S1.5	0.102
2	520542968	19 20 17.61	-47 11 13.5	14.671	0.000			
3	248255370	20 06 19.32	+32 34 11.1	15.068	0.000			
4	145276761	07 38 07.02	+21 27 29.6	15.343	0.000			
5	165172583	23 58 28.23	-22 59 31.8	15.449	0.000			
6	217606410	10 04 16.57	-07 46 34.6	15.581	0.000			
7	618425984	05 02 52.38	-47 13 30.5	15.782	0.000			
8	1280655360	17 00 04.27	-15 16 15.3	15.843	0.000			
9	179865237	05 28 36.55	-15 19 24.8	15.895	0.000			
10	710146476	07 55 34.27	-73 08 02.7	16.161	0.000			
11	396995135	00 10 24.64	+51 52 34.2	13.718	0.001			
12	883197922	13 39 22.92	-54 45 06.6	14.920	0.001			

Table notes: The "W2" sample of moderate-likelihood AGN candidates. Table 5 is published in its entirety in the electronic edition of the Astrophysical Journal, and can also be downloaded from http://www.astro.ucla.edu/~malkan/w2r/table5.xls. A portion is shown here for guidance regarding its form and content. The 2MASS identifier is given in the first column, followed by Right Ascension and Declination in Columns 2 and 3. The measured values of J are given in Column 4, and S_I is given in Column 5. If a source is listed in the VCV catalog, the source name, redshift and identification from that catalog are given in Columns 6-8. The table is sorted primarily by increasing value of S_I and secondarily by increasing J magnitude.

FIGURE CAPTIONS

Figure 1. The five columns give measured 2MASS/WISE colors (J-H, H-K, W1-W2, W2-W3, W3-W4). The first three rows are histograms showing the distribution of these colors for each the three samples considered in this paper (the full sample of 83,510 WISE/2MASS/RASS sources, the 4,954 with SDSS-8 data, and the 741 identified as lines=B). Each histogram has 50 bins. The last row gives *R*, the ratio of counts in the last two histograms. *R* data are plotted for only bins with more than 5 counts in the SDSS histogram.

Figure 2. First four rows are the same format as Figure 1, for the parameterizations S_I, $\log_{10}(S_X)$ and S_{IX} in columns 1-3. The fifth row is the integral probability, that is, the expected success rate for a sample of sources with a parameterization up to a given value. The vertical red dotted lines show where R crosses 0.5 (based on interpolation between the two nearest points) at $S_I = 0.888$, $\log_{10}(S_X) = 0.969$ and $S_{IX} = 0.316$. The cutoff used to define the W2R sample is shown as a green dashed line at $S_{IX} = 0$. Likewise the blue dashed line at $S_I = 1.73$ indicates the cutoff used to derive the W2 sample in Appendix A.

Figure 3. KAST red side spectra (5460-8200 A) of the 7 bright W2R sources not listed in VCV. The spectral response of the detector was removed by dividing the spectra by a flatfield of the illuminated dome ceiling. Thus the flux scale is arbitrary, but does preserve relative slope differences between the spectra. The curvature in some of the continua around 5600 Å is an artifact of inadequate correction for the cutoff of the D55 dichroic. The dotted blue vertical line shows the redshifted wavelength of the strongest expected absorption line, from Na D. The horizontal red dashed lines show the expected locations of the strongest emission lines, Hα, [NII]6584, the [SII]6716/6730 doublet, and [OIII]5007. The telluric absorption in the A and B bands at 6870 and 7650 Å is indicated in green. The Seyfert 1 galaxies are identified in all cases by the broad wings on their strong Hα emission line. The first six sources are clearly broad-line AGN. The last source, W2R 0814-10 has a featureless spectrum; its identification as a BL Lac object is based on a radio source (NVSS J081411-101208) within 2".

Figure 4. Plot of $\log_{10}(S_X)$ vs. S_I for the SDSS sample. Lines=B AGN are shown as red crosses, other (non-AGN) sources are shown as blue x's. The solid black line in the lower left indicates the $S_{IX} = 0$ cutoff; the region below and left of that line has a ~6% contamination with non-AGN. For the RASS-detected objects (lower half of the graph), a less stringent choice of S_I would accept more AGN, while gradually including more contaminants. However there are many AGN which are too X-ray weak for RASS to detect (upper left corner). These are also strongly concentrated to small values of S_I (less than 1). But even adopting the strict cutoff $\log_{10}(S_I) < 0$ still includes a large minority of non-AGN contaminants.

Figure 5. Composition of the W2R sample as a function of J magnitude (top), declination (middle) and absolute value of Galactic latitude (|b|, bottom). The 4,316 sources were ranked and sorted into 26 bins of 166 objects each, and the median of each bin is given on the x-axis. Seyfert 1s/quasars are shown as blue circles, blazars are green x's, non-AGN as red crosses, and unidentified sources as black boxes. Note that the completeness is best for bright, northern sources away from the Galactic plane.

Figure 6. Kast optical spectra of the 13 new AGN in the Kepler field. The left two panels show the blue-side and red-side spectra for 6 objects. The remaining 7 have only their red-side spectra shown, since these have the key broad Balmer line emission which is crucial to identifying the Seyfert 1 (or quasar) nucleus. On the blue side some of these AGN show the CaII HK doublet from stellar absorption. Three at the highest redshifts show broad MgII 2800A line emission. The red dashed lines indicate the redshifted wavelength for various emission lines and the blue dotted lines for absorption lines, as in Figure 3. The source W2R 1926+42 has a featureless spectrum; it is identified as a BL Lac based on a radio source (NVSS J192631+420958) within 2".

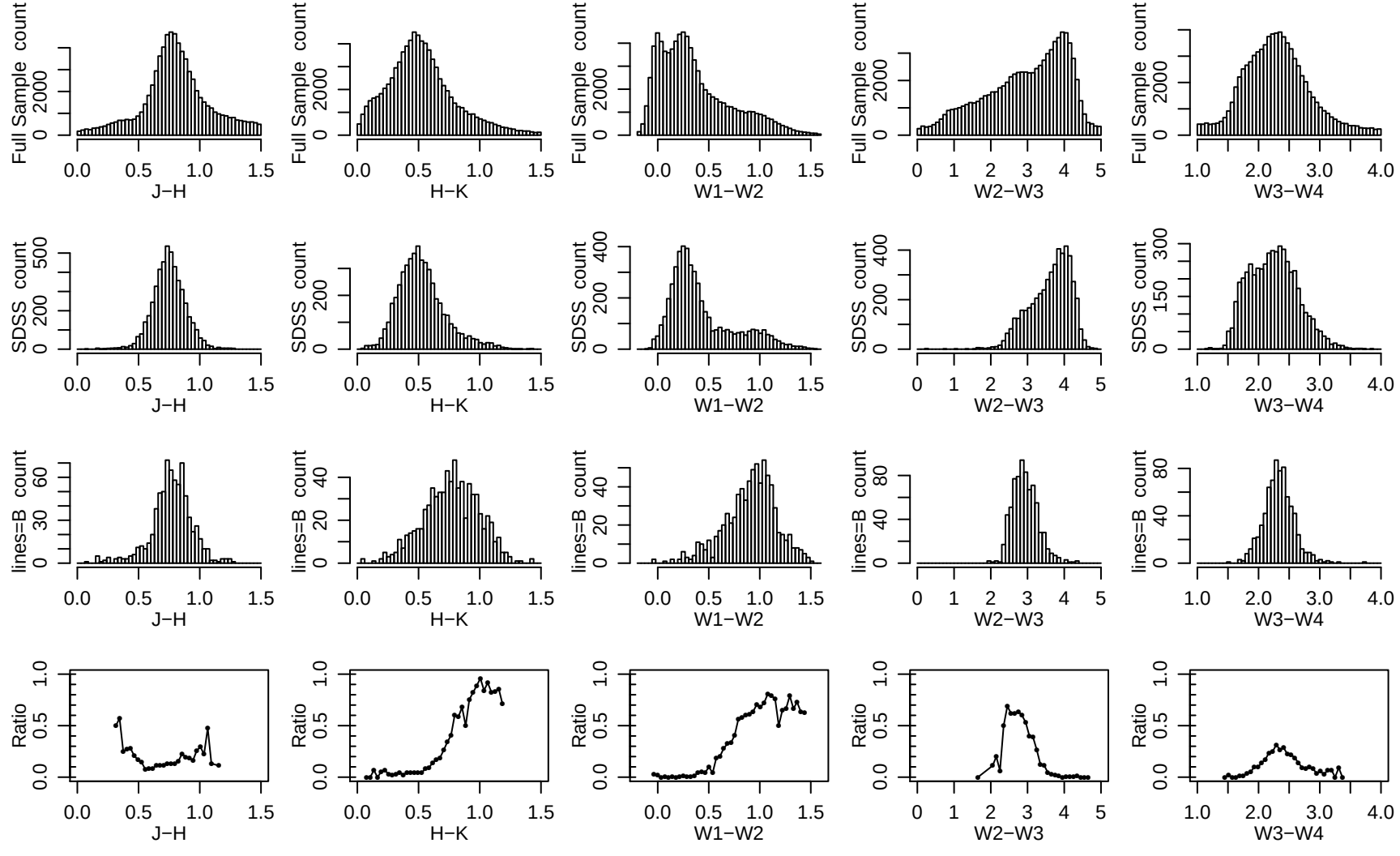
Full Sample count
SDSS count
lines=B count
Ratio
J−H
H−K
W1−W2
W2−W3
W3−W4

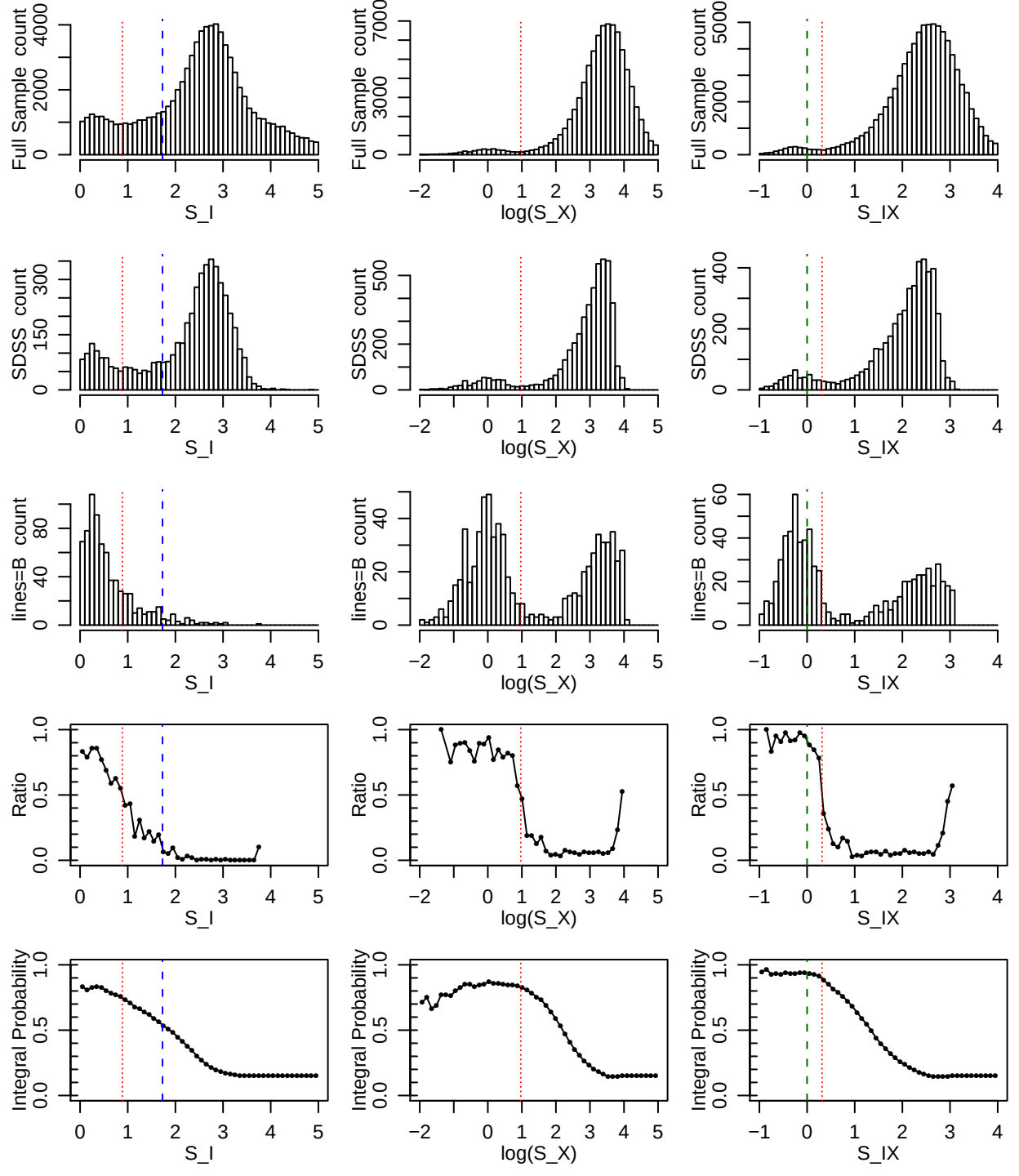
Full Sample count
SDSS count
lines=B count
Ratio
Integral Probability
S_I
log(S_X)
S_IX

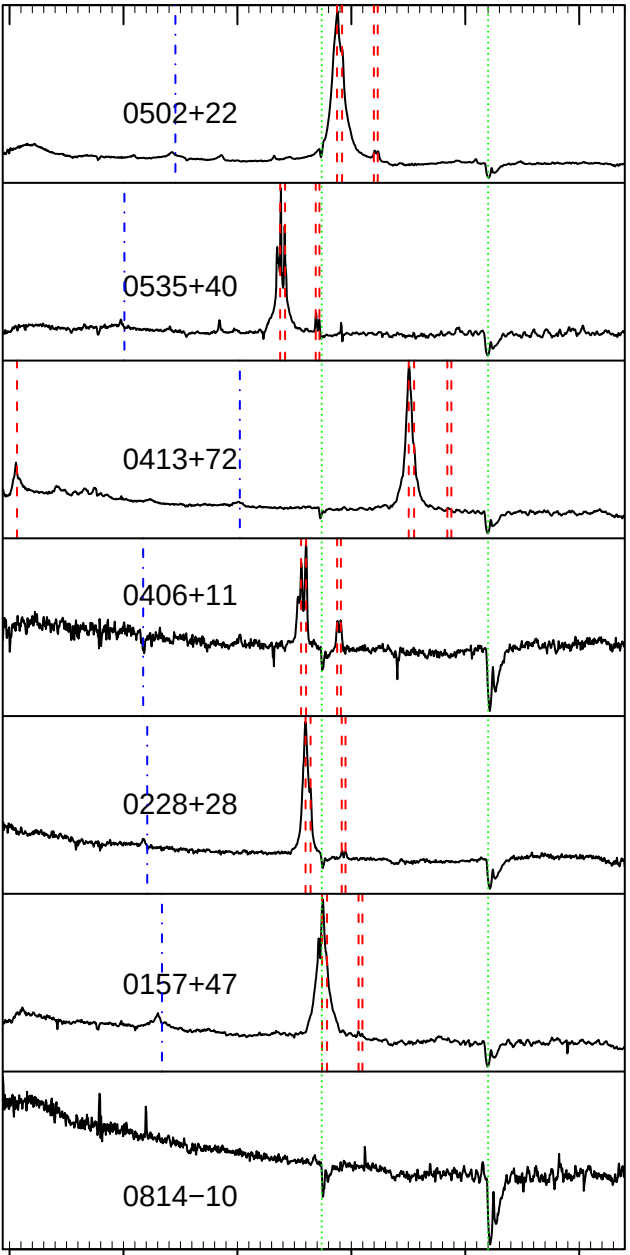
0502+22
0535+40
0413+72
0406+11
0228+28
0157+47
0814−10
5500
6000
6500
7000
7500
8000
Wavelength (A)

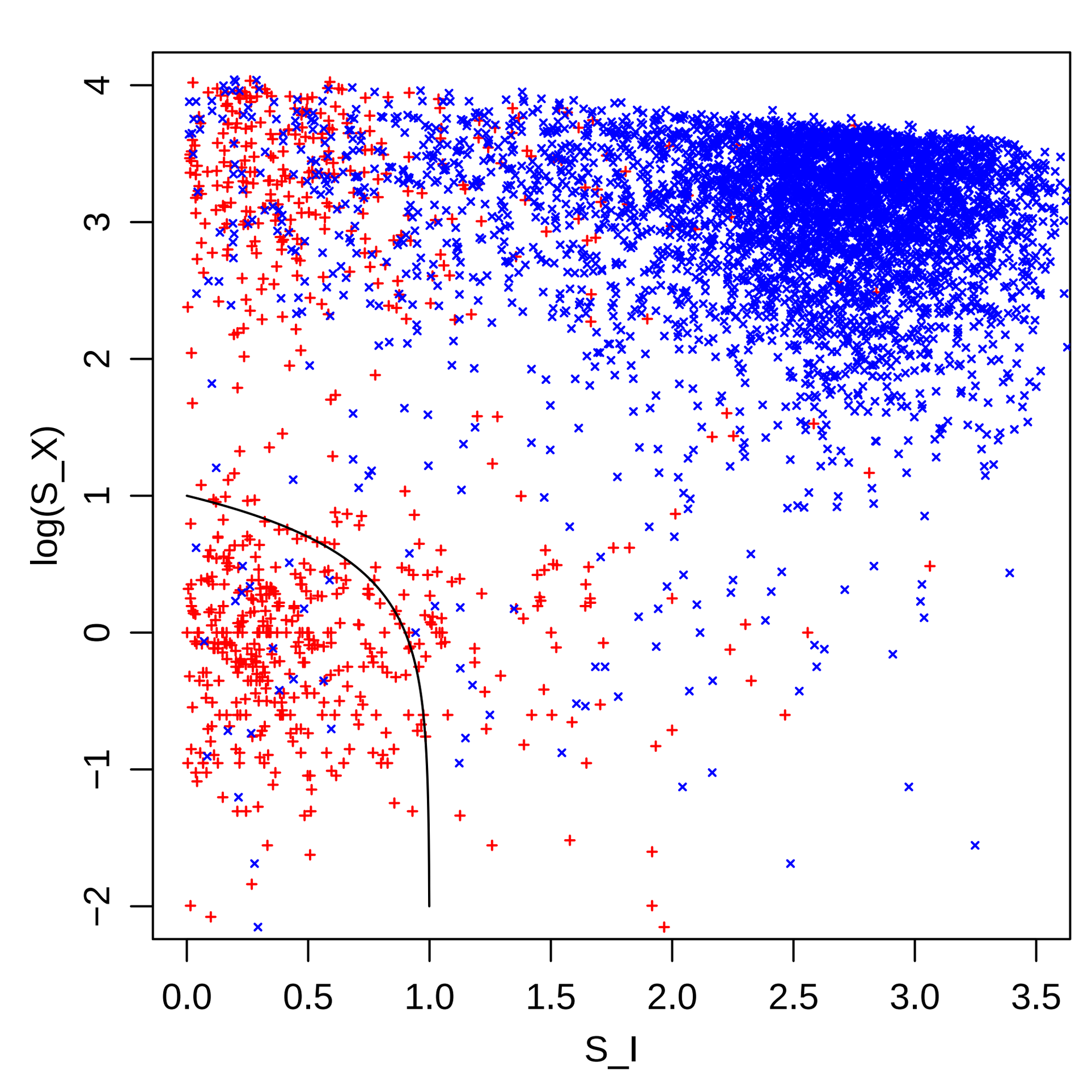
log(S_X)
4
3
2
1
0
−1
−2
0.0
0.5
1.0
1.5
2.0
2.5
3.0
3.5
S_I

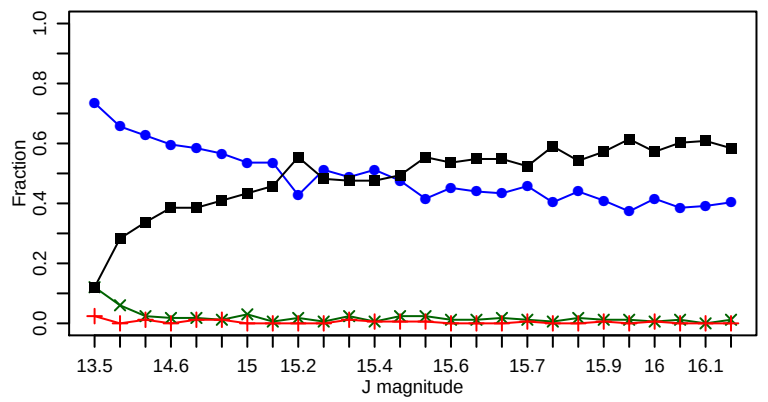
Fraction
0.0
0.2
0.4
0.6
0.8
1.0
13.5
14.6
15
15.2
15.4
15.6
15.7
15.9
16
16.1
J magnitude

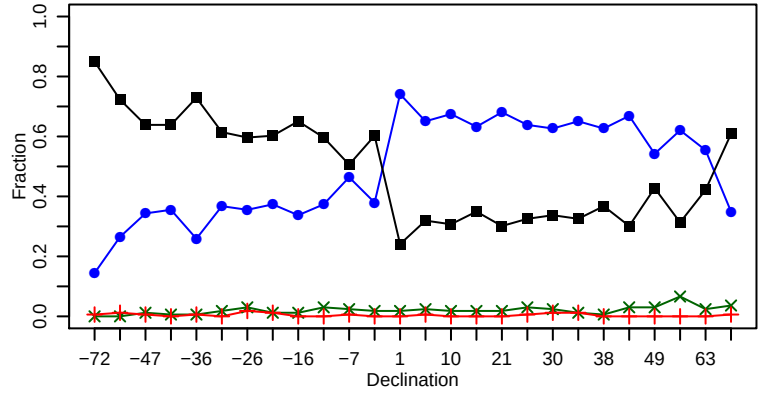
Fraction
0.0
0.2
0.4
0.6
0.8
1.0
−72
−47
−36
−26
−16
−7
1
10
21
30
38
49
63
Declination

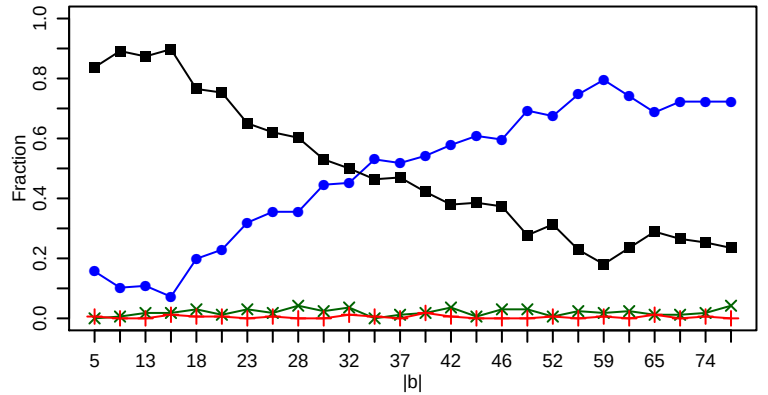
Fraction
0.0
0.2
0.4
0.6
0.8
1.0
5
13
18
23
28
32
37
42
46
52
59
65
74
|b|

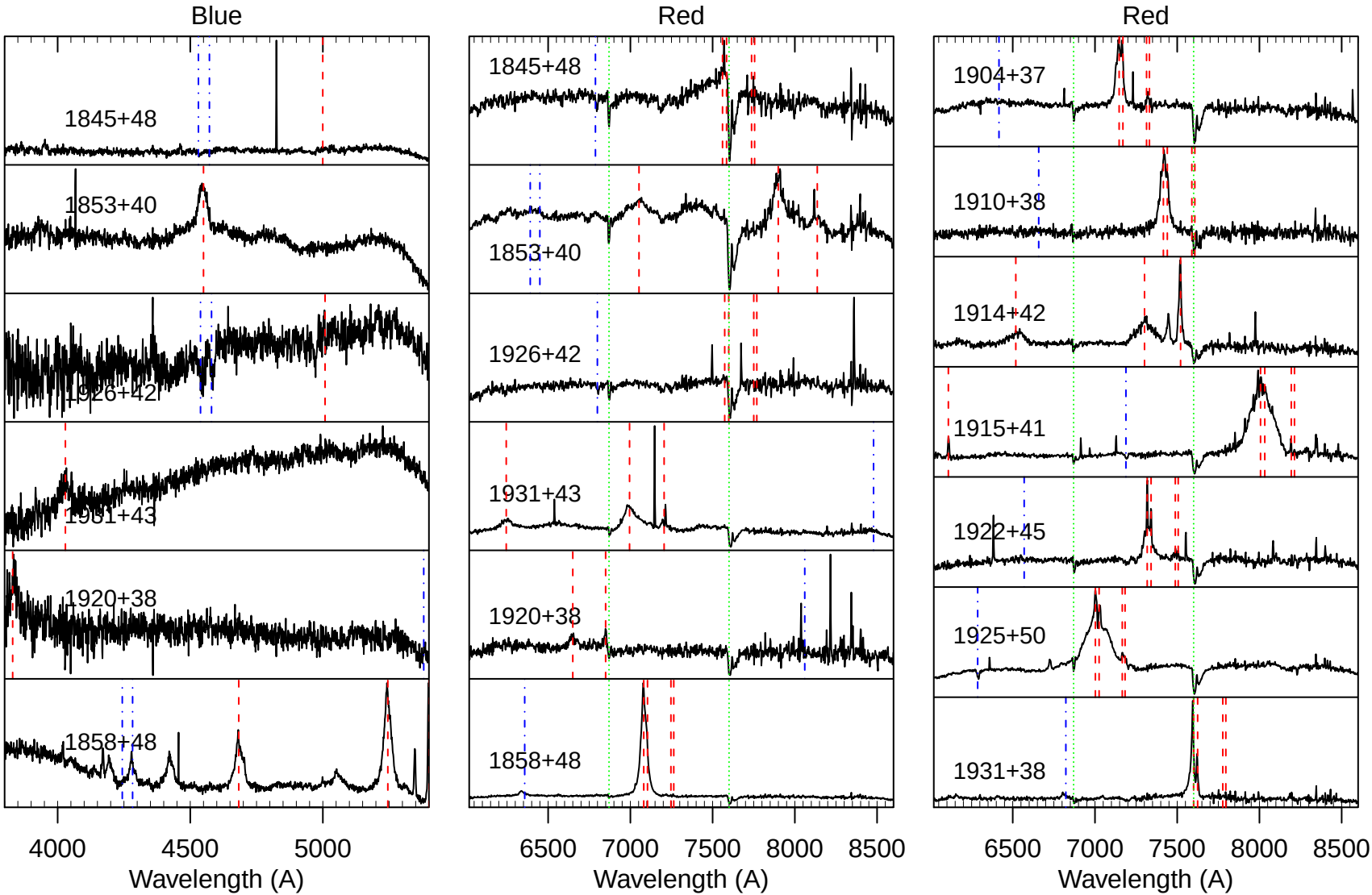
Blue
Red
Red
1845+48
1853+40
1926+42
1931+43
1920+38
1858+48
1845+48
1853+40
1926+42
1931+43
1920+38
1858+48
1904+37
1910+38
1914+42
1915+41
1922+45
1925+50
1931+38
4000
4500
5000
6500
7000
7500
8000
8500
6500
7000
7500
8000
8500
Wavelength (A)
Wavelength (A)
Wavelength (A)